Chinese Journal of Physics 89 (2024) 390–403

Contents lists available at ScienceDirect

Chinese Journal of Physics

journal homepage: www.elsevier.com/locate/cjph

Effects of electron–phonon coupling and Rashba spin–orbit interaction on thermodynamic and magnetic properties of quantum dots

K. Lakaal [a,b], L.M. Pérez [c], M. Kria [a,b], J. El Hamdaoui [a,b], C.O. Edet [d,e], V. Prasad [f], D. Laroze [g], E. Feddi [a,h,*]

[a] Group of Optoelectronic of Semiconductors and Nanomaterials, ENSET, Mohammed V University in Rabat, Morocco
[b] Laboratory of Condensed Matter and Interdisciplinary Sciences (LaMCScI), Faculty of Sciences, Mohammed V-Agdal University, Rabat, Morocco
[c] Departamento de Física, FACI, Universidad de Tarapacá, Casilla 7 D, Arica 1000000, Chile
[d] Department of Physics, Cross River University of Technology, Calabar, Nigeria
[e] Institute of Engineering Mathematics, Universiti Malaysia Perlis, Arau, Perlis, 02600, Malaysia
[f] Department of Physics, Swami Shraddhanand College, University of Delhi, Delhi 110036, India
[g] Instituto de Alta Investigación, CEDENNA, Universidad de Tarapacá, Casilla 7 D, Arica 1000000, Chile
[h] Institute of Applied Physics, Mohammed VI Polytechnic University, Lot 660, Hay Moulay Rachid Ben Guerir, 43150, Morocco

ARTICLE INFO

Keywords:
Polaron
Rashba spin–orbit interaction
Magnetization
Susceptibility
Quantum dot
Wigner parameter

ABSTRACT

The thermodynamic and magnetic properties of quantum-dot structures subjected to an applied magnetic field were studied, including the longitudinal optical–phonon interaction and the Rashba spin–orbit effect. The Schrödinger equation was solved to determine the energy levels. The partition function was evaluated by summing the accessible energy levels and was then utilized to calculate the thermomagnetic functions. In this paper, we present magnetic properties by considering three interacting polarons. Our results indicated that at $B = 0T$, the susceptibility exhibits diamagnetic behavior for all values of the Rashba spin–orbit parameter. However, the magnetic susceptibility increases with an applied magnetic field, and the system exhibits paramagnetic behavior under moderate magnetic fields. However, in situations with and without the polaron effect, the susceptibility is saturated at $0(meV/T^2)$ under large magnetic fields. In this study, we showed that the Rashba spin–orbit interaction (SOI) strengthens the cutoff magnetic field B_c (the B value at which the magnetic nature of the dot changes from diamagnetic to paramagnetic). Rashba SOIs reduce the mean energy of the system, including polaronic interactions. Under the polaron effect, the heat capacity curve shifts to lower temperatures. A quantitative description of the magnetocaloric effect (ΔS) as a function of the Wigner and Rashba spin–orbit parameters is presented.

1. Introduction

In artificially created quantum heterostructures known as quantum dots (QDs), electron motion is restricted to the three spatial dimensions. The energy levels and densities of states of QDs resemble those of atoms and molecules, which are often referred to as artificial atoms/molecules [1]. The past two decades have seen rapid developments in fabrication techniques that have revolutionized

* Corresponding author.
E-mail addresses: lperez@academicos.uta.cl (L.M. Pérez), e.feddi@um5r.ac.ma (E. Feddi).

https://doi.org/10.1016/j.cjph.2023.10.045
Received 4 October 2022; Received in revised form 26 October 2023; Accepted 30 October 2023
Available online 8 November 2023

the physics and engineering of QDs to a level where QDs with almost any desired shape can be grown. Applications in areas such as solar cells [2–5], the development of new laser sources [6,7], and new types of photodetectors [8] have increased the amount of research attention on QDs. As reported previously, the discrete energy-level structure and high values of the transition matrix elements between different levels make them strong candidates for manipulating the structural and responsive properties of QDs [9].

For application-related devices, spin manipulation plays a dominant role in the study of QDs in external magnetic fields. Studies on topological insulators and Weyl fermions are related to spin effects because they are useful in spin Hall-effect analyses, which may provide a tool for spintronic device fabrication [10,11]. The main focus of such studies is spin–orbit interactions (SOIs). Rashba and Dresselhaus are the two main types of SOIs, and they have equal strengths and effects. Spintronic devices are the result of manipulating the electronic spin. SOIs have revealed intriguing changes in various properties; for example, the addition of SOIs significantly affects the magnetic and thermodynamic properties (specific heat, entropy, Helmholtz free energy, etc.). Researchers have demonstrated that spin–orbit effects are highly potent with regard to thermomagnetic properties [12–18]. Recently, we studied the effects of SOIs on the thermomagnetic properties of two electrons in two-dimensional (2D) systems [19]. We showed that Rashba SOIs (RSOIs) increase the cutoff magnetic field B_c (the B value at which the QD's magnetic nature changes from diamagnetic to paramagnetic) with an increase in temperature. In addition, we demonstrate that the polaron effect and RSOIs reduce the mean energy of the system. The SOI has been widely observed in studies on quantum heterostructures over the past two decades. The primary reason for this renewed interest is the fact that in the presence of SOIs, the magneto-optical, magnetocaloric, and even thermoelectric properties of nanostructures can be tuned to the desired level of accuracy [14]. Most studies have focused on a single electron and two electrons in QDs where the confinement is a parabolic or semi-parabolic confining potential. These potentials have attracted attention for two reasons: the analytical solution for most systems under parabolic confinement is readily available, and even for a two-electron system, the center of mass and the relative coordinates can be easily separated, and the problem is reduced to a relative motion equation [20,21]. The mathematical treatment becomes more challenging as the number of interacting electrons increases. Only a few studies have been conducted with three electrons [16,22,23].

Systems with a controlled number of electrons injected into QDs are attracting increasing attention. It has been shown that the number of electrons can influence the SOI and RSOI, which allows regulation of the spin in magnetotransport processes. This technique has exciting prospects for the production of spintronic devices. Potential applications include nonvolatile memory systems [24–28], quantum computing [29], and other spintronic devices [30].

In general, semiconductors have polar or ionic characteristics that influence the physical properties of electrons. This intrinsic polarization induces an electron-longitude-optical (LO) phonon interaction called a *polaron*. Although these interactions are weaker than electron–electron Coulomb interactions, they are similar to SOIs. The importance of these effects on the electronic properties of QDs in the presence of a magnetic field has been extensively investigated. Generally, the Fröhlich formalism is a good framework for studying polaron effects. Within this formalism, two approaches are widely used to solve the Schrödinger equation with phonon terms: the Landau–Pekar [31] or Lee–Low Pines transformations [32]. Huangfu and Yan studied the effects of the magnetic field on the binding energy of a hydrogenic impurity by considering the interactions between electrons and phonons [33]. Melnikov and Fowler [34,35] studied the effects of electron–LO–phonon interactions on the electronic properties of a spherical QD embedded in a nonpolar matrix. Feddi et al. studied the polaron effect on doped spherical QDs under magnetic and electric fields [36–38]. The results of these studies indicated that the energy spectrum, magnetic effect, and polarizability depend strongly on the polaron effect in the weak- and strong-confinement regimes.

The objective of this study was to investigate the thermal and magnetic characteristics of three-electron GaAs QDs in the presence of an external magnetic field, with consideration of the influence of SOIs. The interplay between the magnetization of a material and an applied magnetic field has recently been a subject of considerable interest. In addition, a material search was conducted to examine magnetocaloric effects (MCEs). The MCE, which is often referred to as adiabatic temperature change, causes magnetic materials to heat or cool as a result of changing magnetic fields [39–41]. It is shown that a sudden temperature change (ΔT_{ad}) and change in entropy (ΔS_m) are correlated with the magnetization (M) of the magnetic material, as well as with the heat capacity. Although all magnetic materials are expected to exhibit the MCE, it has not been fully explored in the current literature. The remainder of this paper is organized as follows: Section 1 presents a detailed theoretical model, followed by detailed results and discussions in Section 2, Finally, a brief conclusion is illustrated for the findings of the results.

2. Theoretical formulation

In this section, we present the theoretical approach for determining the thermal and magnetic properties of GaAs in QD systems, with consideration of the electron–LO–phonon interactions. Within the Boltzmann–Gibbs statistical framework, all thermodynamic and magnetic properties are calculated using the canonical partition function defined by $Z_c = \sum_v exp\left(-\beta E_v\right)$, where $\beta = 1/k_B T_a$, k_B is the Boltzmann constant, and T_a represents the temperature in Kelvin (K). Importantly, the summation applies to all system energy levels, E_v is obtained by solving the Schrödinger equation $\hat{H}|v\rangle = E_v|v\rangle$. The mean energy of the system is calculated using the following formula:

$$\langle E\rangle = k_B T_a^2 \frac{\partial \ln Z_c}{\partial T_a}. \tag{1}$$

The heat capacity, which provides information regarding the quantity of energy stored in the system, is evaluated as follows:

$$C_v = -k_B \beta^2 \left(\frac{\partial\langle E\rangle}{\partial\beta}\right). \tag{2}$$

The entropy expression, which is one of the most essential thermodynamic quantities, describes the disorder of a system. It is calculated using the following formula:

$$S = k_B\beta(\langle E\rangle - F_H), \tag{3}$$

where $F_H = -k_B T_a \ln Z_c$ represents the Helmholtz free energy, which constitutes the stability criterion.

From the statistical expressions, the magnetization M can be calculated as

$$M = \frac{-1}{Z_c}\sum_{v}\frac{\partial E_v}{\partial B} exp\left(-\beta E_v\right). \tag{4}$$

Magnetic susceptibility $\chi = \frac{\partial M}{\partial B}$ can be used to determine the degree of magnetization of a material subjected to an applied magnetic field (B). This indicates that the material has diamagnetic ($\chi \prec 0$) or paramagnetic ($\chi \succ 0$) characteristics.

The MCE is the response of the magnetic moments of a magnetic material to the action of an external magnetic field at a particular temperature [42]. Under a varying magnetic field, the MCE provides information on the properties of a magnetic material that can change its temperature or exchange heat with the thermal reservoir. The two quantities used to characterize the MCE are the magnetocaloric potential ΔS and temperature change ΔT_a. Thus, to calculate the magnetic entropy change ΔS, the entropy is first evaluated in the presence and absence of a magnetic field. The quantity ΔS for an isothermal process is given as [41]

$$\Delta S = S(B \neq 0, T_a) - S(B = 0, T_a). \tag{5}$$

These thermodynamic quantities require *knowledge* of the energy spectrum of the system. First, we determined the energy of three interacting electrons confined in a QD with an applied perpendicular magnetic field $\vec{B} = (0, 0, B)$, which is described in the symmetric gauge by $\vec{A} = \frac{1}{2}(\vec{B}\times\vec{r})$. Taking into account the effect of the RSOI, the energy of the three correlated polarons is a solution to the Schrödinger equation $\hat{H}|v\rangle = E_v|v\rangle$. In the effective mass approximation, considering the Zeeman and RSOI effects, the Hamiltonian can be expressed as

$$\hat{H} = \hat{H}_{el} + V_c + \hat{H}_R^{SO} + \hat{H}_z + \hat{H}_{pol}, \tag{6}$$

Here, the first term represents the Hamiltonian of the three interacting electrons in a QD under the confinement potential, which is supposed to be parabolic and is given by

$$\hat{H}_{el} = \frac{1}{2m_e^*}\sum_{j=1}^{3}\left(\vec{p}_j + \frac{e\vec{A}_j}{c}\right)^2 + \frac{1}{2}m_e^*\omega_0^2\sum_{j=1,i<j}^{3}\left|\vec{r}_j - \vec{r}_i\right|^2, \tag{7}$$

where m_e^* represents the effective mass of the electron, e represents the electron charge, c represents the speed of light in vacuum, $\overrightarrow{p_j}$ represents the momentum of the electron (j), and $\hbar\omega_0$ represents the energy scale of the parabolic confinement.

The second term of Eq. (6) represents the electron–electron interaction, which is defined as

$$V_c = \sum_{j=1}^{3}\sum_{i=1}^{j-1}\frac{e^2}{\epsilon_\infty\left|\vec{r}_j - \vec{r}_i\right|}, \tag{8}$$

where ϵ_∞ is the high-frequency dielectric constant.

The Rashba spin–orbit Hamiltonian is given by the third term in Eq. (6), which is expressed as follows:

$$\hat{H}_R^{SO} = \frac{\alpha_R}{\hbar}\sum_{j=1}^{3}\left[\hat{\sigma_j}\times\left(\hat{p_j} + \frac{e\hat{A}_j}{c}\right)\right] = \frac{\alpha_R}{\hbar}\sum_{i=1}^{3}\left[\hat{\sigma}_{x,i}(\hat{p}_{y,i} + \frac{e\hat{A}_{y,i}}{c}) - \hat{\sigma}_{y,i}(\hat{p}_{x,i} + \frac{e\hat{A}_{x,i}}{c})\right], \tag{9}$$

where $\hat{\sigma} = (\hat{\sigma_x}, \hat{\sigma_y}, \hat{\sigma_z})$ are the Pauli matrices and α_R denotes the Rashba coupling constant.

In Eq. (6), the fourth term denotes the Zeeman effect.

$$\hat{H}_z = \frac{1}{2}g^* B\mu_B\sum_{j=1}^{3}\hat{\sigma}_{z,j}, \tag{10}$$

where $\mu_B = \frac{e\hbar}{2m_0 c}$ denotes the Bohr magneton, and g^* is the Lande factor of the electron.

The rightmost term in Eq. (6) is the kinetic operator of the phonon and the electron–LO–phonon coupling, which is described in the framework of the Fröhlich approach [43]. This approach is explained using a simple image. Indeed, in a polar semiconductor, when an electron in the conduction band moves in a material characterized by its Coulomb field, ionic polarization is produced around it, which influences the electronic movement. Under these conditions, the particle must acquire polarization during movement. This quasiparticle, which is formed by an electron and the induced polarization charge, is called a polaron. In the Fröhlich approach, the optical modes have the same frequency. The dielectric is treated as a continuous medium, and the electrons move with a quadratic dispersion. Using this approach, the last terms in Eq. (6) can be expressed as

$$\hat{H}_{pol} = \sum_{\vec{q}}\hbar\omega_{LO}\hat{a}_{\vec{q}}^{+}\hat{a}_{\vec{q}} + \sum_{\vec{q}}\sum_{j=1}^{3}\left[\hat{a}_{\vec{q}}V_{\vec{q}}\exp(i\vec{q}\vec{r_j}) + H.c\right]. \tag{11}$$

Here, ω_{LO} represents the LO-phonon frequency, $\hat{a}^{+}_{\vec{q}}(\hat{a}_{\vec{q}})$ denotes the phonon's creation (annihilation) operator with a $3D$ wave vector $\vec{q} = (\vec{q}_{\parallel}, \vec{q}_z)$ in the optical branch, and $V_{\vec{q}}$ is the coefficient of electron–LO–phonon coupling, which is given by the following formula [43]:

$$V_{\vec{q}} = \left[\frac{2\pi e^2}{V}\frac{\hbar\omega_{LO}}{q^2}\left(\frac{1}{\varepsilon_\infty} - \frac{1}{\varepsilon_0}\right)\right]^{1/2}, \tag{12}$$

where V represents the volume of the crystal.

Recall that in $(III - IV)$ semiconductors characterized by weak electron–phonon coupling, interactions with phonons can be considered through a polaronic mass depending on the electron–LO–phonon coupling α_{LO}. According to the Feynman approximation for weak electron–LO–phonon coupling [44],

$$m_p^* = m_e^*(1 + \frac{\alpha_{LO}}{6}). \tag{13}$$

with

$$\alpha_{LO} = \frac{e^2}{2\hbar\omega_{LO}}\left(\frac{2m_e^*\omega_{LO}}{\hbar}\right)^{1/2}\left(\frac{1}{\varepsilon_\infty} - \frac{1}{\varepsilon_0}\right). \tag{14}$$

To solve the Schrödinger equation $\hat{\mathcal{H}}|\nu\rangle = E_\nu|\nu\rangle$, we first introduce the Jacobi coordinates as follows [45]: $\overrightarrow{R} = \frac{\vec{r}_1 + \vec{r}_2 + \vec{r}_3}{3}$, $\vec{\rho} = \frac{\vec{r}_1 - \vec{r}_2}{\sqrt{2}}$ and $\vec{\lambda} = \frac{\vec{r}_1 + \vec{r}_2 - 2\vec{r}_3}{\sqrt{6}}$ for the coordinates and $m_e^* = m_\rho^* = m_\lambda^*$ and $M_e = 3m_e^*$ for the masses. Thus, the Hamiltonian of Eq. (6) becomes

$$\hat{\mathcal{H}} = \hat{\mathcal{H}}_0 + V_c + \hat{\mathcal{H}}_{pol}. \tag{15}$$

The three parts of the previous Hamiltonian are the total Hamiltonian of the non-interacting electrons obtained after motion separation, the Coulomb potential, and the Hamiltonian representing the electron–LO–phonon coupling. These terms are defined as follows:

$$\hat{\mathcal{H}}_0 = \frac{p_\rho^2}{2m_\rho^*} + \frac{p_\lambda^2}{2m_\lambda^*} + \frac{1}{2}m_e^*\Omega^2(\rho^2 + \lambda^2) + \frac{P_R^2}{2M_e} + \frac{1}{8}M_e\omega_c^2R^2 + \frac{1}{2}\omega_c\sum_{j=1}^{3}L_z^{(j)} + \frac{\alpha_R}{\hbar}\begin{pmatrix} 0 & \mathcal{H}_{12} \\ \mathcal{H}_{21} & 0 \end{pmatrix} + \frac{3}{2}g^*\mu_B B\begin{pmatrix} 1 & 0 \\ 0 & -1 \end{pmatrix}, \tag{16}$$

$$V_c = \frac{e^2\eta}{\varepsilon_\infty\sqrt{\rho^2 + \lambda^2}}, \tag{17}$$

where $\Omega^2 = \frac{\omega_c^2}{4} + 3\omega_0^2$ with $\omega_c = \frac{eB}{m_e^*c}$ represents the Larmor frequency, $L_z = m\hbar(m'\hbar)$ denotes the angular momentum's z-component in the center of mass (CM) part (relative part), m and m' denote the CM and relative part's angular momentum quantum numbers, respectively, which can take the values $0, \pm1, \pm2...$, and $\eta = \left[\frac{\sqrt{1+\alpha^2}}{\alpha\sqrt{2}} + \frac{\sqrt{2(1+\alpha^2)}}{\sqrt{3}+\alpha} + \frac{\sqrt{2(1+\alpha^2)}}{\sqrt{3}-\alpha}\right]$.

with, $\alpha = \frac{\rho}{\lambda}$, and $\mathcal{H}_{12}$, and $\mathcal{H}_{21}$ are developed from the Rashba operator term's matrix element, which is given as

$$\begin{cases} \mathcal{H}_{12} = \hbar\left[\frac{\partial}{\partial R_x} - i\frac{\partial}{\partial R_y}\right] + eB(R_x - iR_y) \\ \mathcal{H}_{21} = \hbar\left[-\frac{\partial}{\partial R_x} - i\frac{\partial}{\partial R_y}\right] + eB(R_x + iR_y) \end{cases} \tag{18}$$

Given the conditions described above, the Hamiltonian is separated into two independent parts, i.e., $\hat{\mathcal{H}} = \hat{\mathcal{H}}_{rel} + \hat{\mathcal{H}}_{CM}$, and the energy spectrum of the system is expressed as $E = E_{rel} + E_{CM}$. The Schödinger equation describing the relative motion is defined as follows (see Appendix):

$$\frac{d^2U_{n',m'}(\xi)}{d\xi^2} - \left[\beta^2\xi^2 + \frac{2e^2\eta}{\varepsilon\hbar\omega_0\sqrt{\frac{\hbar}{m_p^*\omega_0}}\xi} + \frac{\tilde{\ell}(\tilde{\ell}+2) + \frac{3}{4}}{\xi^2}\right]U_{n',m'}(\xi) = \left(\frac{m'\omega_c}{\omega_0} - \varepsilon_{n',m'}\right)U_{n',m'}(\xi) \tag{19}$$

where $\beta^2 = 3 + \frac{\omega_c^2}{4\omega_0^2}$, $\xi^2 = \frac{m_p^*\omega_0}{\hbar}(\rho^2 + \lambda^2)$, $\varepsilon_{n',m'} = \frac{2E_{rel}}{\hbar\omega_0}$ and n', $\tilde{\ell}$, and m' are three quantum numbers.

Eq. (19) can be solved using a previously reported method [16,46,47]. The relative motion energy of the system, which is expressed in units of $\frac{\hbar\omega_0}{2}$, is

$$\varepsilon_{n',m'} = 2\left(n' + \frac{1}{2}\right)\sqrt{\frac{1}{2}\frac{d^2V_{eff}(\xi)}{d\xi^2}\Big/_{\xi=\xi_0}} + V_{eff}(\xi)\Big/_{\xi=\xi_0} + \frac{m'\omega_c}{\omega_0}, \tag{20}$$

Here, $V_{eff}(\xi) = \beta^2\xi^2 + \frac{2R_W'}{\xi} + \frac{\tilde{\ell}(\tilde{\ell}+2)+\frac{3}{4}}{\xi^2}$, with $R_W' = \frac{e^2\eta}{\varepsilon\hbar\omega_0 l_0}$ being the Wigner parameter, which represents the relative strength of the Coulombic repulsion between two electrons separated by a distance of $l_0 = \sqrt{\frac{\hbar}{m_e^*\omega_0}}$ and twice the electron's zero-point kinetic energy moving into harmonic confinement.

Table 1
The *GaAs* material parameters used in this study were extracted from [23,48,49].

Material	$\frac{m_e^*}{m_0}$	E_g(eV)	ϵ_0	ϵ_∞	R'_W	$\hbar\omega_{LO}$(meV)	$\hbar\omega_{TO}$(meV)	α_R(meV × nm)
GaAs	0.067	1.42	12.53	10,90	(1–10)	36,7	33,29	(1–5.4)

For center-of-mass motion, the time-independent Schrödinger equation is expressed as follows:

$$-\frac{\hbar^2}{2M_e}\left[\frac{\partial^2}{\partial R_x^2}+\frac{\partial^2}{\partial R_y^2}\right]\Psi_n(R,\Phi)+\frac{1}{2}M_e\Omega^2R^2\Psi_n(R,\Phi)+\frac{1}{2}\omega_c L_Z\Psi_n(R,\Phi)$$
$$+\frac{\alpha_R}{\hbar}\begin{pmatrix}0 & H_{12}\\ H_{21} & 0\end{pmatrix}\Psi_n(R,\Phi)+\frac{3}{2}g^*\mu_B B\begin{pmatrix}1 & 0\\ 0 & -1\end{pmatrix}\Psi_n(R,\Phi)=E_{CM}\Psi_n(R,\Phi). \tag{21}$$

By selecting $R_x = Rcos\Phi$, $R_y = Rsin\Phi$, $R^2 = R_x^2 + R_y^2$, and $\Phi = \arctan\left(\frac{R_y}{R_x}\right)$, the following expressions for $\mathcal{H}_{12}$ and $\mathcal{H}_{21}$ given in Eq. (18) can be obtained:

$$\begin{cases}\mathcal{H}_{12}=\hbar e^{-i\Phi}\left[\frac{\partial}{\partial R}-\frac{i}{R}\frac{\partial}{\partial\Phi}+\frac{eBR}{c}\right]\\ \mathcal{H}_{21}=\hbar e^{+i\Phi}\left[-\frac{\partial}{\partial R}-\frac{i}{R}\frac{\partial}{\partial\Phi}+\frac{eBR}{c}\right]\end{cases} \tag{22}$$

By considering the wave function as the product of independent angular and radial terms, we obtain

$$\Psi_{n,m}(R,\Phi)=\begin{cases}U_n(R)e^{im\Phi}\\ V_n(R)e^{i(m+1)\Phi}\end{cases} \tag{23}$$

Under these conditions, the Hamiltonian takes the following form [19]:

$$\left\{\begin{array}{l}\left(\frac{\partial^2}{\partial R^2}+\frac{1}{R}\frac{\partial}{\partial R}+k^2-\frac{m^2}{R^2}\right)U_n(R)-\frac{M_e\omega_c^2R^2}{4\hbar^2}U_n(R)-\frac{2M_e\alpha}{\hbar^2}\left(\frac{\partial}{\partial R}+\frac{m+1}{R}\right)V_n(R)-\frac{2M_e\alpha RBe}{\hbar^3}V_n(R)=0\\ \left(\frac{\partial^2}{\partial R^2}+\frac{1}{R}\frac{\partial}{\partial R}+q^2-\frac{(m+1)^2}{R^2}\right)V_n(R)-\frac{M_e\omega_c^2R^2}{4\hbar^2}V_n(R)-\frac{2M_e\alpha}{\hbar^2}\left(-\frac{\partial}{\partial R}+\frac{m}{R}\right)U_n(R)-\frac{2M_e\alpha RBe}{\hbar^3}U_n(R)=0\end{array}\right\} \tag{24}$$

where n and m represent the principal and magnetic quantum numbers, respectively, of the different CM states, $k^2=\frac{-M_e m\omega_c}{\hbar}-\frac{3M_e g^*\mu_B B}{\hbar^2}+\frac{2M_e}{\hbar^2}E_{CM}$, and $q^2=\frac{-M_e(m+1)\omega_c}{\hbar}+\frac{3M_e g^*\mu_B B}{\hbar^2}+\frac{2M_e}{\hbar^2}E_{CM}$.

To solve Eq. (24), we use the following wave functions for the CM, which is expressed as a linear combination of Bessel functions:

$$\begin{cases}U_n(R)=AJ_m(kR)+BJ_m(qR)\\ V_n(R)=AJ_{m+1}(kR)+BJ_{m+1}(qR)\end{cases} \tag{25}$$

We only consider the fundamental state of the CM motion, which corresponds to $n = 1$ and $m = 0$. Then, the energy eigenvalues E_{CM} can be calculated via the numerical solution of the above differential equations $\hat{H}_{CM}\Psi_n(R,\Phi)=E_{CM}\Psi_n(R,\Phi)$.

3. Numerical results and discussion

Our numerical calculations are applied to the GaAs QDs. Table 1 presents all the physical parameters used in this study, taken from the references cited herein. To determine the relative strengths of the SOI and confinement, the following two length scales are used: $l_s=\sqrt{\frac{\hbar^2}{2m_e^*\alpha_R}}$ and $l_0=\sqrt{\frac{\hbar}{m_e^*\omega_0}}$, where l_s represents the length corresponding to the SOI, and l_0 represents the characteristic length of the confinement potential.

We focused primarily on the three-electron GaAs QD. The approach mentioned in the Theoretical Formulation section was used to determine the energy levels of the three-electron QD in an applied magnetic field with the RSOI. As discussed in the previous section, the energy corresponding to a three-electron system is given as $E = E_{CM} + E_{rel}$, where the E_{CM} expression includes the RSOI term. It is well known that the levels' degeneracy is lifted because of α_R. Zeeman splitting occurs even in the absence of the SOI, and the results are not shown here; however, they are analogous to those found in [9,18], and the level splitting in our case is significantly more pronounced.

From the numerical calculations performed in this study, which are presented in Table 2, the temperature (T_a) and magnetic field (B) affect the saturation of the summation in the expression Z_c. At $T_a = 100$ K, Z_c is saturated from the 12th level for $B = 15$ T and at the 22nd level for $B = 10$ T. In contrast, for $B = 5$ T, it reaches saturation at the 26th level. However, saturation was reached toward the end of more states for $T_a = 300$ K. We infer that, Z_c is saturated at the 140th, 190th, and 198th levels for $B = 15$ T, $B = 10$ T, and $B = 5$ T, respectively.

In Fig. 1, the effective potential is plotted as a function of ξ with different values of the Wigner parameter ($R'_W = 0, 1, 5$, and 10). The figure illustrates the dependence of the effective potential on the Wigner parameter. With an increase in the Wigner parameter,

Table 2
Partition function with varying magnetic fields and energy levels at T_a = 100 K and T_a = 300 K.

$B(T)$	5	10	15
		Z_c at T_a = 100 K	
N = 12	3.840192736E−5	7.181002597E−6	7.537266032E−7
22	3.867508285E−5	7.211805687E−6	7.537266032E−7
26	3.867512407E−5	7.211805687E−6	7.537266032E−7
29	3.867512407E−5	7.211805687E−6	7.537266032E−7
		Z_c at T_a = 300 K	
N = 140	0.1528546460	8.265973191E−2	3.609030166E−2
190	0.1535412371	8.294744409E−2	3.609030166E−2
198	0.1535412379	8.294744409E−2	3.609030166E−2
200	0.1535412379	8.294744409E−2	3.609030166E−2

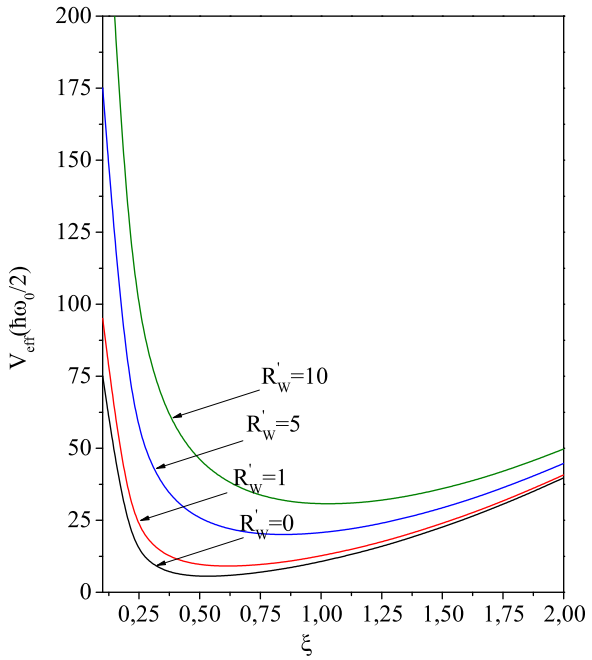

Fig. 1. Plot of the effective potential with respect to ξ for different values of the Wigner parameter ($R'_W = 0, 1, 5,$ and 10).

the minimum effective potential shifts to larger values of ξ. However, the effective potential converges to almost the same value for all the Wigner parameter values.

Magnetic susceptibility (χ) is a crucial parameter that defines the degree of magnetization of the system. It also defines the diamagnetic or paramagnetic characteristics of a material. Its determination allowed us to determine possible magnetic transitions.

Fig. 2 shows the magnetic susceptibility (χ) of the GaAs QD with respect to the magnetic field strength, which is given by the ratio ω_c/ω_0 at T_a = 1 K. To study the effects of the RSOI, the results for two cases with and without the RSOI were examined, as shown in Fig. 2a. It is well known that the susceptibility is always negative if the RSOI is neglected (α_R = 0) (shown in the inset of Fig. 2a), and it is positive in the case where the RSOI is nonzero (α_R = 1, 2, and 5.4 meV nm). This implies that the RSOI reinforces the susceptibility. Interestingly, at ω_c/ω_0 = 0 (B = 0 T), the figure shows diamagnetic behavior ($\chi \prec 0$) for each value of the RSOI (α_R = 1, 2, and 5.4 meV nm) in both cases, i.e., with and without consideration of electron–LO–phonon interactions. However, considering the configuration where electron–LO–phonon interactions are nonzero, the susceptibility is far higher than that in the case where this interaction is ignored. In both cases, the susceptibility increases with the magnetic field strength, and the system exhibits paramagnetic behavior ($\chi \succ 0$) at an intermediate magnetic field strength. In addition, it can be said that the susceptibility is saturated at $0(eV/T^2)$ under strong magnetic fields. It was also observed that RSOI shifted the curves to stronger magnetic fields. As shown in Fig. 2b, (χ) with respect to ω_c/ω_0 was studied in the case where the RSOI was neglected for various Wigner parameter values ($R'_W = 0, 1, 5,$ and 10). Interestingly, the susceptibility is negative (diamagnetic behavior) for all values of the Wigner parameter. The figure also shows that R'_W increases χ.

The magnetization M given by Eq. (4) refers to the ability of the sample to maintain induced magnetism when a magnetic field is applied.

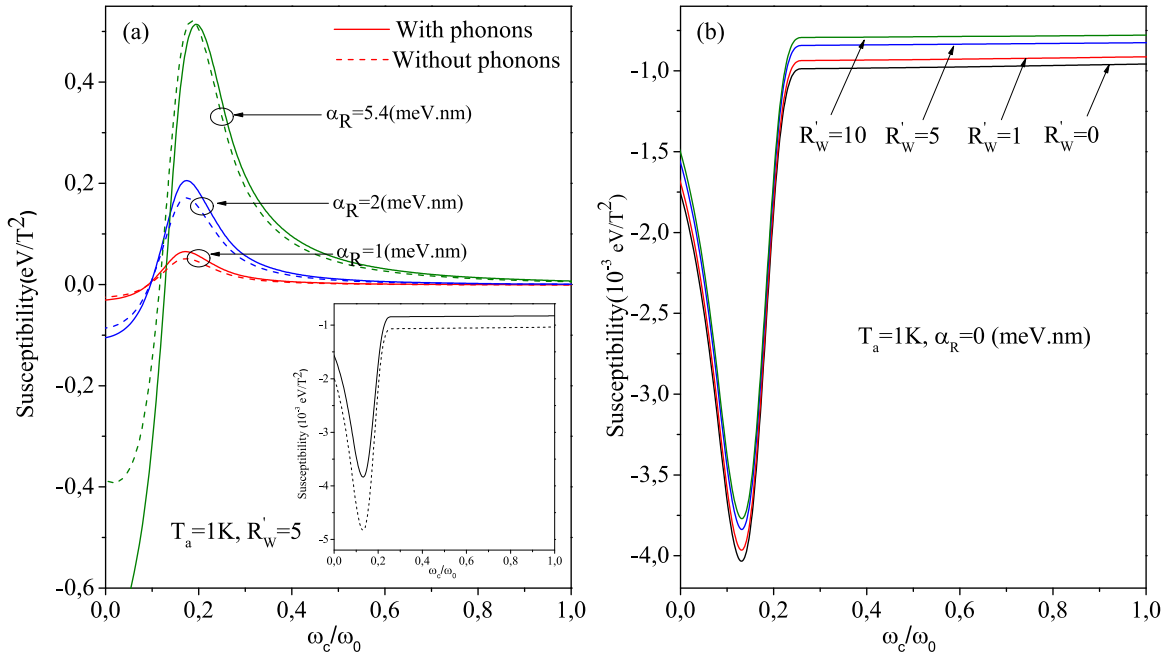

Fig. 2. Susceptibility as a function of ω_c/ω_0 (a) with four values of the RSOI, i.e., $\alpha_R = 0, 1, 2$, and 5.4 meV nm, at $R'_W = 5$ (the solid and dotted lines correspond to the cases with and without the polaron effect, respectively) and (b) for various Wigner parameter values: $R'_W = 0, 1, 5$, and 10. All the curves are plotted for phonons at $T_a = 1$ K.

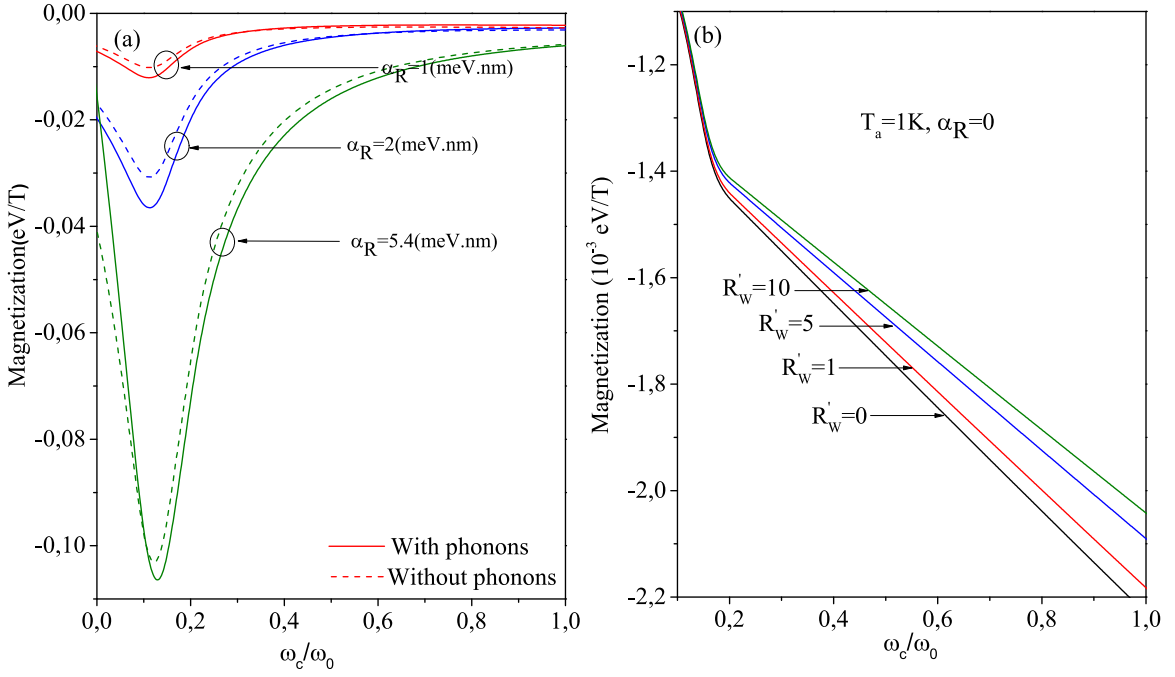

Fig. 3. Plot of the magnetization for GaAs vs. ω_c/ω_0 (a) with three values of the RSOI, i.e., $\alpha_R = 1, 2$, and 5.4 meV nm, at $R'_W = 5$ (the solid and dotted lines correspond to the cases with and without the polaron effect, respectively) and (b) for various Wigner parameter values $R'_W = 0, 1, 5$, and 10. All the curves are plotted for phonons at $T_a = 1$ K.

The variation in magnetization M with respect to the frequency ratio $\frac{\omega_c}{\omega_0}$ is shown in Fig. 3. The solid and dotted lines correspond to the cases with and without the polaron effect, respectively. To study the effect of the RSOI, the magnetization (M) for various values of the RSOI ($\alpha_R = 1, 2$, and 5.4 meV nm) at $R'_W = 5$ was examined, as shown in Fig. 3a. In both cases, i.e., with and without

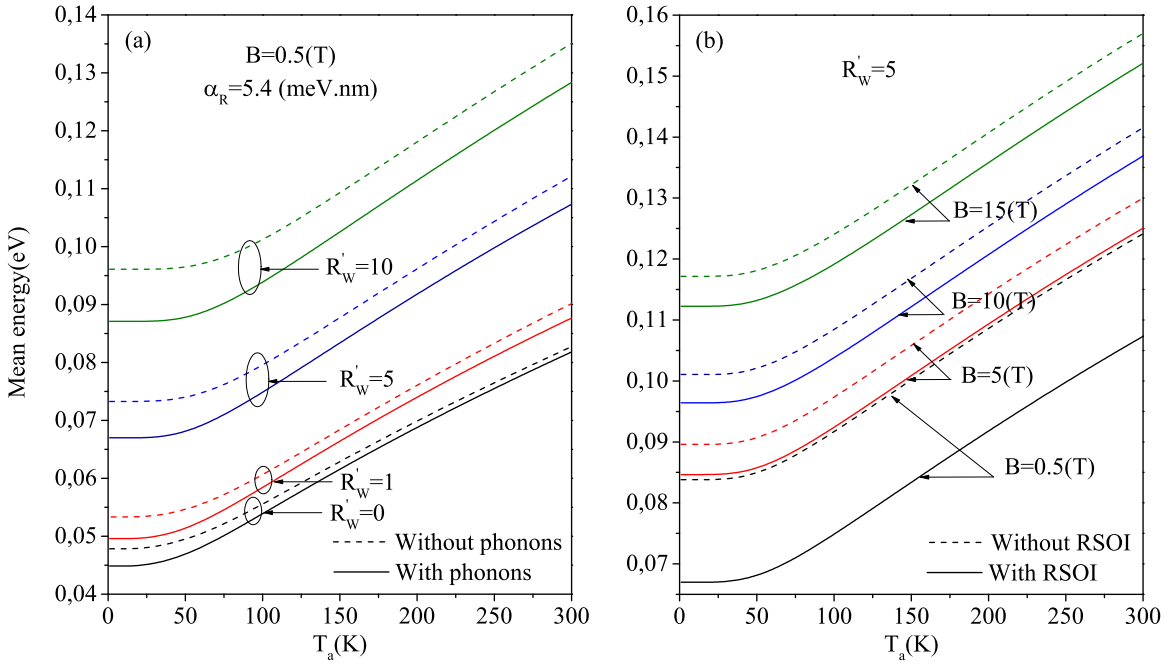

Fig. 4. Mean energy of the GaAs QD vs. the temperature (a) with and without phonons for various Wigner parameter values (R'_W, 1, 5, and 10) at $\alpha_R = 5.4$ meV nm and $B = 0.5$ T and (b) without and with the RSOI for four values of the magnetic field, i.e., $B = 0.5, 5, 10$, and 15 T, at $R'_W = 5$.

electron–phonon interactions, there are essentially two regions: the first is located at $\frac{\omega_c}{\omega_0} \lesssim 0.1$ ($B \lesssim 0.19$ T). When the magnetic field strength increases, the magnetization tends to decrease. The second region is located at $\frac{\omega_c}{\omega_0} \gtrsim 0.1$ ($B \gtrsim 0.19$ T), and the magnetization increases with the magnetic field strength. We also notice that for a given B, the system marks the reinforcement of magnetization with a decreasing RSOI value.

Interestingly, these results indicate that the magnetization generally decreases toward a minimum afterward, fluctuates, and then increases until a saturation value is reached. Following this definition, the slope of the magnetization is described by the susceptibility $\chi = \frac{dM}{dB}$ in the (M, B) diagram, as shown in Fig. 3a. The magnetization diminishes before the minimum is reached ($\frac{dM}{dB} < 0$), implying that the system has diamagnetic behavior ($\chi < 0$). From this minimum, the magnetization starts to increase and exhibits a positive slope ($\frac{dM}{dB} > 0$), which implies that the system has paramagnetic behavior ($\chi > 0$).

As shown in Fig. 3b, the magnetization (M) vs. ω_c/ω_0 graph in the case where the RSOI is not considered for various Wigner parameter values ($R'_W = 0, 1, 5$, and 10) was studied in the presence of electron–LO–phonon interactions. The first observation made here is that the magnetization has a negative value, and for a given temperature value ($T_a = 1K$), the magnitude of magnetization (M) decreases when the magnetic field strength increases, which signifies the diamagnetic character of the material ($\chi < 0$). The figure also shows that as the magnetic field and R'_W increase, M increases. Additionally, at a very low B, M is independent of R'_W. This agrees with the results of [13,16,19,50].

By using the partition function Z_c with respect to the temperature and magnetic field strength, the thermodynamic properties of this system are discussed, taking into account electron–LO–phonon coupling. The variation in the mean energy of the GaAs QD as a function of the temperature is shown in Fig. 4. As the temperature increases, the mean energy of the system increases. This is because the kinetic energy of the system becomes more important as the temperature increases.

Similarly, to better understand the R'_W effect on the mean energy, we examined the variation in the mean energy for GaAs with respect to the temperature for various Wigner parameter values ($R'_W = 0, 1, 5$, and 10) in two cases with and without electron–LO–phonon interaction at $\alpha_R = 5.4$ meV nm and $B = 0.5$ T, as shown in Fig. 4a. The mean energy increases with the interaction strength (from $R'_W = 0$ to $R'_W = 10$). It can be posited that the electron–LO–phonon interactions reduce the mean energy of the system.

The variation in the mean energy as a function of the temperature with different magnetic field strengths ($B = 0.5, 5, 10$, and 15 T) at $R'_W = 5$ is shown in Fig. 4b. With an increase in the magnetic field strength, the mean energy of the system increases. The RSOI reduces the mean energy of the system.

Fig. 5a presents a plot of the heat capacity C_V with respect to the temperature, incorporating the effect of the Wigner parameter at $\alpha_R = 5.4$ meV nm and $B = 0.5$ T and taking into account the electron–LO–phonon coupling. As shown, for high temperatures ($T_a > 125K$), the heat capacity of the QD is saturated and is increased significantly by increasing the interaction strength (from $R'_W = 0$ to $R'_W = 10$). At all temperatures, the effect of the electron–LO–phonon interactions on the heat capacity is evident.

Fig. 5b displays the variation in the heat capacity of the GaAs QD as a function of the temperature for different magnetic field strengths $B = 0.5, 5, 10$, and 15 T at $\alpha_R = 5.4$ meV nm and $R'_W = 5$. At low temperatures, an increase in the magnetic field strength reduced C_V; however, at higher temperatures, the magnetic field increased the heat capacity.

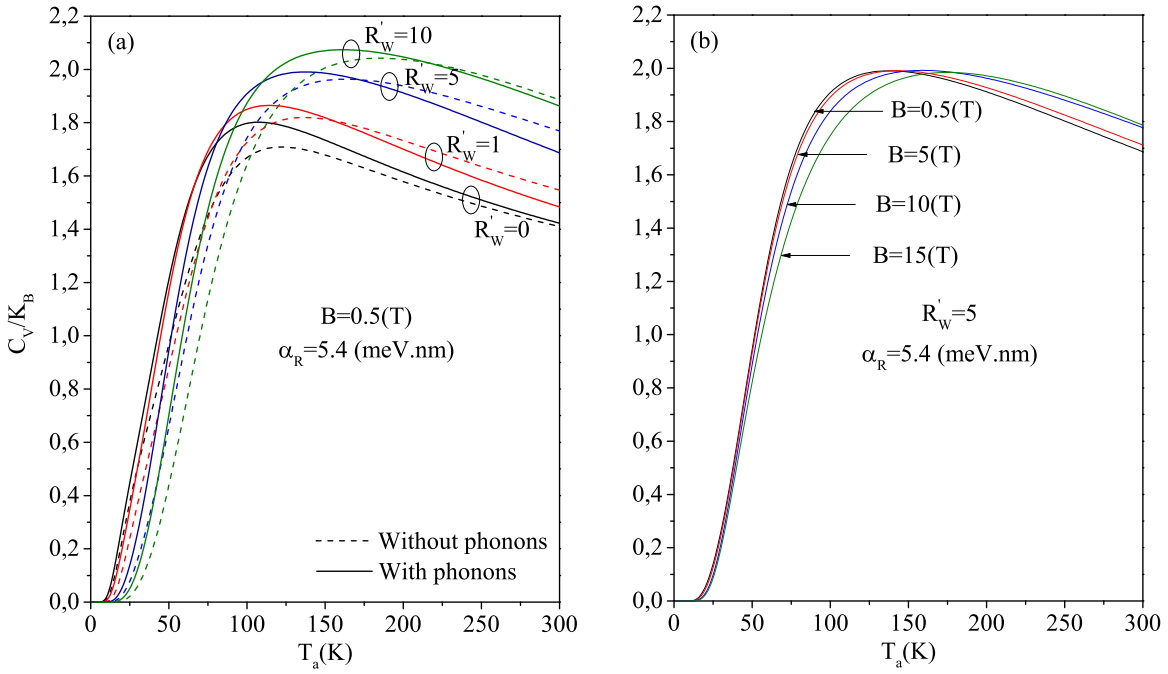

Fig. 5. Heat capacity of the GaAs QD vs. the temperature (a) with and without phonons for various Wigner parameter values, i.e., $R'_W = 0, 1, 5$, and 10, at $\alpha_R = 5.4$ meV nm and $B = 0.5$ T and (b) for four values of the magnetic field, i.e., $B = 0.5, 5, 10$, and 15 T, at $\alpha_R = 5.4$ meV nm and $R'_W = 5$.

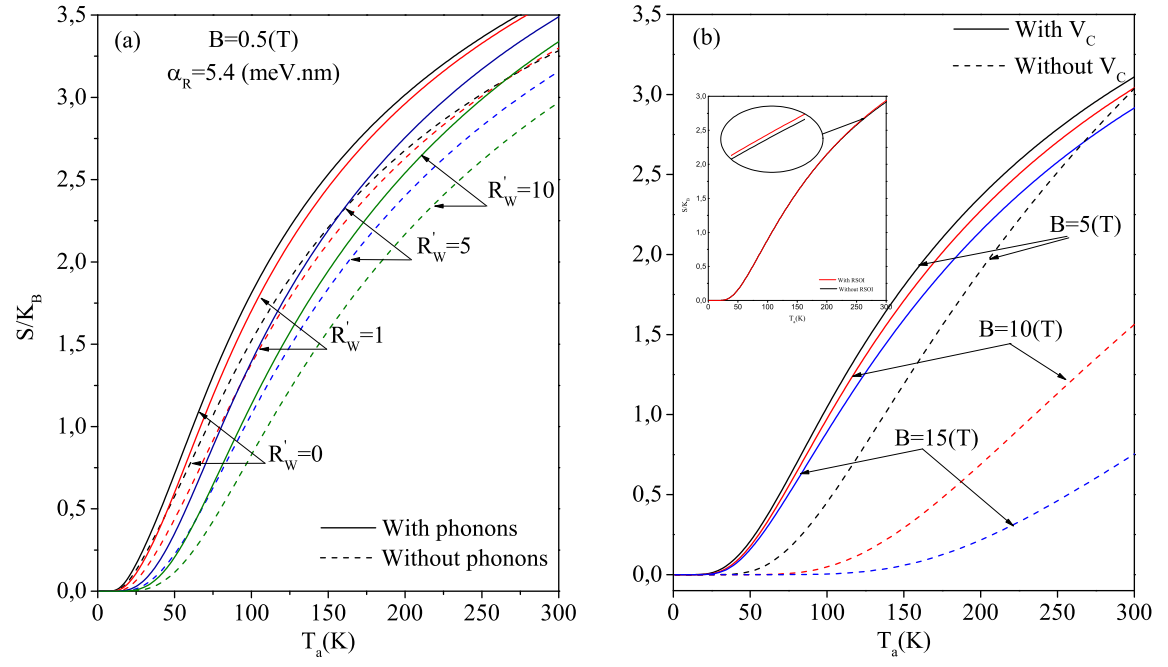

Fig. 6. (a) Plot of entropy for GaAs vs. the temperature with and without phonons for various Wigner parameter values ($R'_W = 0, 1, 5$, and 10) at $B = 0.5$ T. (b) Variation in the entropy as a function of the temperature for three interacting electrons (solid lines) and non-interacting electrons (dashed lines) for different magnetic field strengths ($B = 5, 10$, and 15 T). The inset shows the Rashba effect on the entropy (the red line corresponds to $\alpha_R = 5.4$ meV nm, and the black line corresponds to $\alpha_R = 0$ meV nm). (For interpretation of the references to color in this figure legend, the reader is referred to the web version of this article.)

The variation in the entropy (S) as a function of temperature is shown in Fig. 6. This function, which describes the system disorder, is zero at very low temperatures, according to the laws of thermodynamics. Entropy increases with temperature because

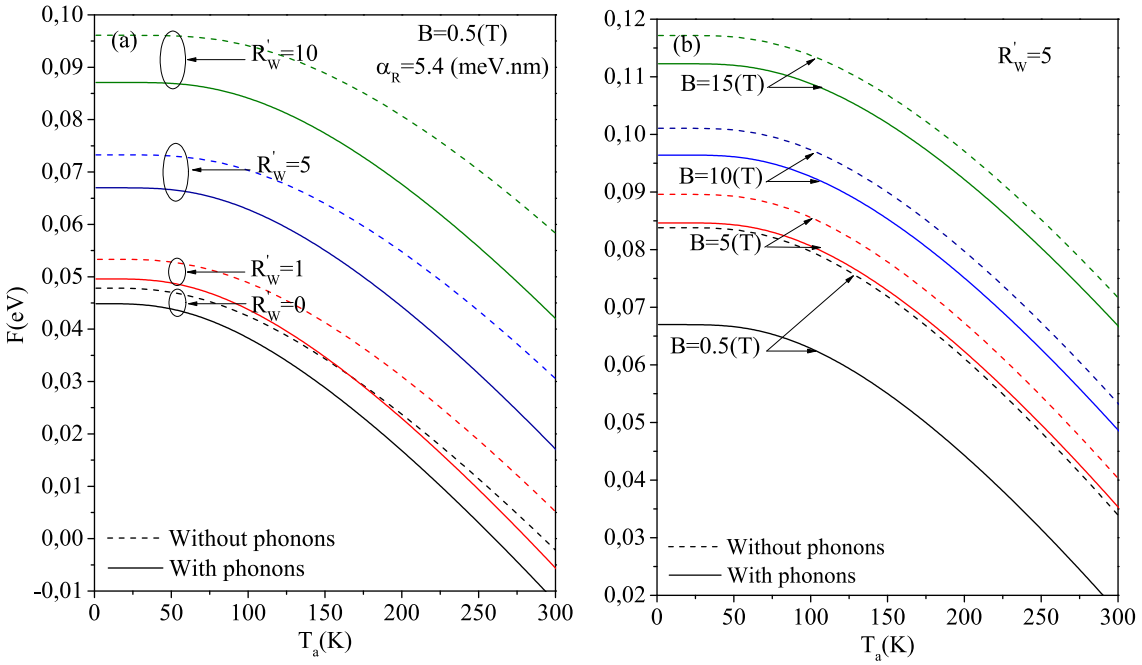

Fig. 7. Helmholtz free energy of the GaAs QD vs. the temperature (a) with and without phonons for various Wigner parameter values, i.e., $R'_W, 1, 5$, and 10, at $\alpha_R = 5.4$ meV nm and $B = 0.5$ T and (b) with and without the RSOI for various magnetic field strengths, i.e., $B = 0.5, 5, 10$, and 15 T, at $R'_W = 5$.

the occupancy probabilities of the levels change, and the disorder of the system becomes important as a result of thermal agitation. Fig. 6a shows the variation in entropy for GaAs with respect to the temperature for various Wigner parameter values ($R'_W = 0, 1, 5$, and 10) and for $B = 0.5$ T. With an increase in R'_W (from $R'_W = 0$ to $R'_W = 10$), the entropy decreases, and the effect of the electron–LO–phonon effect on the entropy is significant at high temperatures.

Fig. 6b shows the variation in the entropy as a function of the temperature for three interacting electrons (solid lines) and non-interacting electrons (dashed lines) for different magnetic field strengths ($B = 5, 10$, and 15 T). The inset shows the Rashba effect on the entropy (the red line corresponds to $\alpha_R = 5.4$ meV nm, and the black line corresponds to $\alpha_R = 0$ meV nm). Our results indicate that at low temperatures, the magnetic field has a weak effect on the entropy. In contrast, at high temperatures, when the disorder of the system becomes important, the application of a magnetic field can align the electron spins, reducing the entropy. To complete our discussion, we analyzed the effect of the RSOI on the entropy of the system. The windows in Fig. 6b show the entropy variations in both cases: with and without the RSOI. The entropy of the system increases when the RSOI is stronger, and the same behavior was reported by Malik et al. [14]. Our computational approach shows that when T_a approaches zero, the RSOI does not affect the entropy, in accordance with the laws of thermodynamics. To clarify the effect of the Coulombic interaction on the system stability, we examined the variation in the entropy as a function of temperature for three interacting and three non-interacting electrons confined in the QD, as shown in Fig. 6b. We compared the behaviors for three different magnetic field strengths ($B = 5, 10$, and 15 T) and considered the RSOI. The entropy of the non-interacting electrons is less pronounced than that of the interacting system, implying that the electrostatic repulsive interactions destabilize the three-electron system.

The Helmholtz free energy contains information regarding the useful work of a system provider. It is defined as the energy necessary to create a system with constant volume and temperature, which provides the stability criterion. Fig. 7 illustrates the variation in the Helmholtz free energy of the GaAs QD with respect to the temperature. In all the curves shown in Fig. 7, the Helmholtz free energy decreases as the temperature increases, which causes the entropy to increase; thus, the Helmholtz free energy decreases. Fig. 7a shows the variation in the Helmholtz free energy of the GaAs QD with respect to the temperature, taking into consideration the effects of the interaction strength (R'_W) and electron–LO–phonon interaction. The results indicate that the Helmholtz free energy strongly depends on the strength of the interaction. It is evident that R'_W increases the Helmholtz free energy. Thus, the interaction strength cannot be neglected. We also see that the electron–LO–phonon interactions reduce the Helmholtz free energy of the system.

In Fig. 7b, the variation in the Helmholtz free energy as a function of temperature with various magnetic field strengths, i.e., $B = 0.5, 5, 10$, and 15 T, at $R'_W = 5$, taking into account the RSOI, is presented. According to the results, the Helmholtz free energy is more important for a higher confinement strength. Additionally, we see that the RSOI reduces the Helmholtz free energy of the system.

Fig. 8 presents the variation in the entropy change (ΔS) as a function of the temperature. It shows the changes in the strength of the magnetic field from $B_i = 0.01$ T to $B_f = 5$ T. In Fig. 8a, the effect of the Wigner parameter R'_W on the entropy change (ΔS)

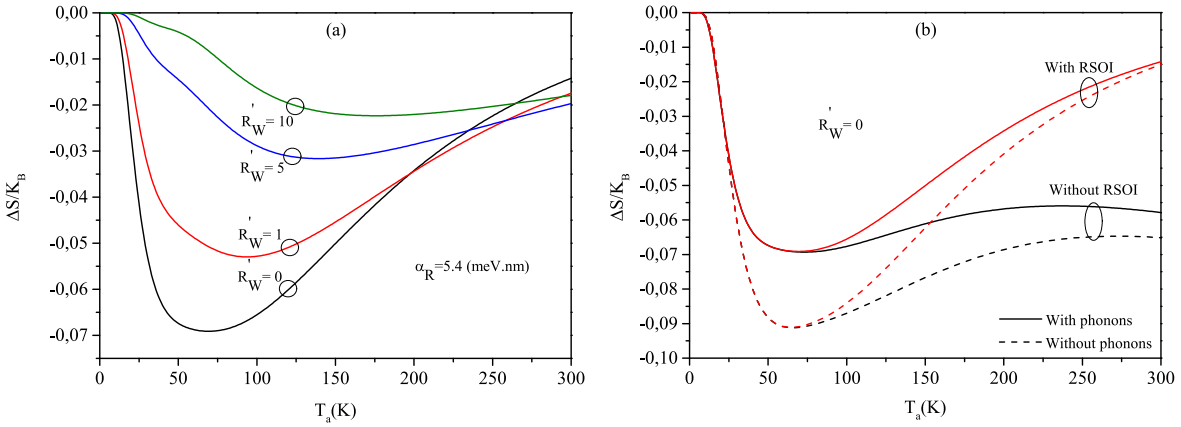

Fig. 8. MCE with respect to the temperature (a) for various Wigner parameter values, i.e., $R'_W, 1, 5$, and 10 (all curves are plotted for phonons at $\alpha_R = 5.4$ meV nm) and (b) with and without the RSOI, considering the effects of electron–phonon interactions.

at $\alpha_R = 5.4$ meV nm is presented. The general behavior of the MCE shows that the entropy changes ΔS decrease toward a minimum afterward, changes its variation, and starts to increase again with increasing temperature until it becomes saturated at a limit value. The figure also shows that when the parameter R'_W increases, the minimum shifts to higher temperatures, and the entropy change increases. Fig. 8b presents the variations in the entropy (ΔS) vs. the temperature with and without the RSOI, in the presence of the electron–LO–phonon interactions. As shown, at low temperatures, the entropy change has the same behavior for both cases (with and without RSOI); however, at higher temperatures, the effect of the RSOI on the entropy change is remarkable. Additionally, electron–phonon interactions reduce the entropy change of the system.

4. Final remarks

We analyzed the magnetic and thermal properties of a three-electron QD. The significance of the present study can be evaluated by considering all the potential electron interactions, including the electron–electron Coulomb interactions, the SOIs, and, most importantly, the electron–phonon interactions. The electron–LO–phonon interactions were assumed to have the same strength as the Rashba or Dresselhaus SOI. These polaronic contributions significantly affect the magnetic and thermal properties of the QD. *An increase in* the number of electrons in the QD increases the Coulomb repulsion terms in the Hamiltonian, and the Coulomb terms dominate the dynamics. However, the polaron effects are still significant, as indicated by all the results. Additionally, polaron effects dominate at low magnetic field strengths, as observed for magnetic susceptibility (Fig. 2a) and magnetization (Fig. 3a). The effect of electron–phonon coupling is far more significant for higher values of the RSOI at low magnetic field strengths. The results presented herein are imperative for future experimental studies aimed at developing new devices for spintronics.

Declaration of competing interest

The authors confirm that they do not have any conflict of interest in connection to this investigation.

Acknowledgments

LMP acknowledges financial support from the ANID, Chile through Convocatoria Nacional Subvención a Instalación en la Academia Convocatoria Año 2021, Grant SA77210040. DL acknowledges financial support from the Centers of Excellence with BASAL/ANID, Chile financing, AFB220001,CEDENNA.

Appendix

This section describes the procedure for calculating the energy levels and wave functions of the system. According to the Eqs. (16) and (17), the total Hamiltonian after the motion separation for the three interacting electrons is expressed as follows:

$$\mathcal{H} = \frac{P_\rho^2}{2m_\rho^*} + \frac{P_\lambda^2}{2m_\lambda^*} + \frac{1}{2}m_e^*\Omega^2(\rho^2+\lambda^2) + \frac{P_R^2}{2M_e} + \frac{1}{8}M_e\omega_c^2R^2 + \frac{1}{2}\omega_c\sum_{j=1}^{3}L_z^{(j)} + \frac{e^2\eta}{\varepsilon\sqrt{\rho^2+\lambda^2}}$$
$$+\frac{\alpha_R}{\hbar}\begin{pmatrix} 0 & H_{12} \\ H_{21} & 0 \end{pmatrix} + \frac{3}{2}g^*\mu_B B\begin{pmatrix} 1 & 0 \\ 0 & -1 \end{pmatrix}. \tag{26}$$

We use the hyperspherical coordinates characterized by the hyperradius ζ and hyperangle κ, which are defined as follows:

$$\zeta^2 = \rho^2 + \lambda^2,\ \kappa = \arctan\left(\frac{\rho}{\lambda}\right) \tag{27}$$

Under these transformations, the first and second terms of Eq. (26) are expressed as follows:

$$\frac{P_\rho^2}{2m_\rho^*} + \frac{P_\lambda^2}{2m_\lambda^*} = -\frac{\hbar^2}{2m_e^*}\left(\frac{\partial^2}{\partial\zeta^2} + \frac{3}{\zeta}\frac{\partial}{\partial\zeta} - \frac{\tilde{\ell}(\tilde{\ell}+2)}{\zeta^2}\right). \tag{28}$$

Therefore, the Hamiltonian describing the relative motion is defined as

$$\mathcal{H}_{rel} = -\frac{\hbar^2}{2m_e^*}\left(\frac{\partial^2}{\partial\zeta^2} + \frac{3}{\zeta}\frac{\partial}{\partial\zeta} - \frac{\tilde{\ell}(\tilde{\ell}+2)}{\zeta^2}\right) + \frac{1}{2}m_e^*\Omega^2\zeta^2 + \frac{e^2\eta}{\varepsilon\zeta} + \frac{l_z}{2}\omega_c \tag{29}$$

With this approach, the Schrödinger equation that describes the relative motion is given as

$$\left[-\frac{\hbar^2}{2m_e^*}\left(\frac{\partial^2}{\partial\zeta^2} + \frac{3}{\zeta}\frac{\partial}{d\zeta} - \frac{\tilde{\ell}(\tilde{\ell}+2)}{\zeta^2}\right) + \frac{1}{2}m_e^*\Omega^2\zeta^2 + \frac{e^2\eta}{\varepsilon\zeta} + \frac{l_z}{2}\omega_c\right]\phi_{n',m'}(\zeta,\kappa) = E_{rel}\phi_{n',m'}(\zeta,\kappa) \tag{30}$$

where the hyperradial wavefunction is given by $\phi_{n',m'}(\zeta,\kappa) = \frac{e^{im'\kappa}}{\sqrt{2\pi}}f_{n',m'}(\zeta)$

We consider the following transformation [46]: $f_{n',m'}(\zeta) = \zeta^{-\frac{3}{2}}U_{n',m'}(\zeta)$. Then, Eq. (30) is reduced to the form

$$\frac{\partial^2 U_{n',m'}(\zeta)}{\partial\zeta^2} + \left[\frac{2m_e^*}{\hbar^2}E_{rel} - \left(\frac{m_e^{*2}\Omega^2\zeta^2}{\hbar^2} + \frac{m_e^*m'\hbar}{2}\omega_c + \frac{2m_e^*}{\hbar^2}\frac{e^2\eta}{\varepsilon\zeta} + \frac{\tilde{\ell}(\tilde{\ell}+2)}{\zeta^2} + \frac{3}{4\zeta^2}\right)\right]U_{n',m'}(\zeta) = 0 \tag{31}$$

When the independent variable $\xi = \sqrt{\frac{m_e^*\omega_0}{\hbar}}\zeta$ is changed, the above equation yields

$$\frac{\partial^2 U_{n',m'}(\xi)}{d\xi^2} - \left[\beta^2\xi^2 + \frac{2e^2\eta}{\varepsilon\hbar\omega_0\sqrt{\frac{\hbar}{m_e^*\omega_0}}\xi} + \frac{\tilde{\ell}(\tilde{\ell}+2)+\frac{3}{4}}{\xi^2}\right]U_{n',m'}(\xi) = \left(\frac{m'\omega_c}{\omega_0} - \frac{2E_{rel}}{\hbar\omega_0}\right)U_{n',m'}(\xi) \tag{32}$$

We set $\varepsilon_{n',m'} = \frac{2E_{rel}}{\hbar,\omega_0}$ and $R_W' = \frac{e^2\eta}{\varepsilon\hbar\omega_0 l_0}$.
Thus, we obtain

$$\frac{\partial^2 U_{n',m'}(\xi)}{d\xi^2} - \left[\beta^2\xi^2 + \frac{2R_W\eta}{\xi} + \frac{\tilde{\ell}(\tilde{\ell}+2)+\frac{3}{4}}{\xi^2}\right]U_{n',m'}(\xi) = \left(\frac{m'\omega_c}{\omega_0} - \varepsilon_{n',m'}\right)U_{n',m'}(\xi) \tag{33}$$

In the previous equation, the effective potential is defined as follows:

$$V_{eff}(\xi) = \beta^2\xi^2 + \frac{2R_W'}{\xi} + \frac{\tilde{\ell}(\tilde{\ell}+2)+\frac{3}{4}}{\xi^2} \tag{34}$$

with $R_W' = R_W\eta$

Furthermore, Taylor expansion of $V_{eff}(\xi)$ yields

$$V_{eff}(\xi) = V_{eff}(\xi)/_{\xi=\xi_0} + \frac{1}{2}\frac{d^2V_{eff}(\xi)}{d\xi^2}/_{\xi=\xi_0}(\xi-\xi_0)^2 \tag{35}$$

$$\frac{\partial^2 U_{n',m'}(\xi)}{\partial\xi^2} - \Omega_{m'}^2(\xi-\xi_0)^2U_{n',m'}(\xi) = \left(\frac{m'\omega_c}{\omega_0} - \varepsilon_{n',m'} + V_{eff}(\xi)/_{\xi=\xi_0}\right)U_{n',m'}(\xi) \tag{36}$$

Here, $\Omega_{m'}^2 = \frac{1}{2}\frac{d^2V_{eff}(\xi)}{d\xi^2}/_{\xi=\xi_0}$.
The well-known Schrödinger equation for a one-dimensional harmonic oscillator is given by

$$\frac{\partial^2\psi(x)}{\partial x^2} - \left(\frac{\mu'\omega'}{\hbar}\right)^2x^2\psi(x) = -\frac{2\mu'\epsilon'}{\hbar^2}\psi(x) \tag{37}$$

whose energy eigenvalues are $\epsilon' = \left(n'+\frac{1}{2}\right)\hbar\omega'$.
A comparison between Eqs. (36) and (37) yields the following correspondence:
$\Omega_{m'}^2 = \left(\frac{\mu'\omega'}{\hbar}\right)^2$ and $\frac{m'\omega_c}{\omega_0} - \varepsilon_{n',m'} + V_{eff}(\xi)/_{\xi=\xi_0} = -\frac{2\mu'\epsilon'}{\hbar^2}$
Therefore, the energy is finally given by

$$\varepsilon_{n',m'} = 2\left(n'+\frac{1}{2}\right)\sqrt{\frac{1}{2}\frac{d^2V_{eff}(\xi)}{d\xi^2}/_{\xi=\xi_0} + V_{eff}(\xi)/_{\xi=\xi_0}} + \frac{m'\omega_c}{\omega_0} \tag{38}$$

References

[1] Q. Zhao, R. Han, A.R. Marshall, S. Wang, B.M. Wieliczka, J. Ni, J. Zhang, J. Yuan, J.M. Luther, A. Hazarika, G.-R. Li, Colloidal quantum dot solar cells: Progressive deposition techniques and future prospects on large area fabrication, Adv. Mater. 34 (2022) 2107888, http://dx.doi.org/10.1002/adma, (29pp).

[2] W.U. Huynh, J.J. Dittmer, A.P. Alivisatos, Hybrid nanorod-polymer solar cells, Science 295 (2012) 2425–2427, http://dx.doi.org/10.1126/science.1069156.

[3] M. Courel, P. Beltran-Bobadilla1, F.J. Sanchez-Rodriguez, I. Montoya De Los Santos, M. Ojeda1, A. Carrillo-Osuna, Hugo J. Cortina-Marrero, L. Hechavarria-Difur, L.M. Pérez, D. Laroze, A proposal to enhance SnS solar cell efficiency: the incorporation of SnSSe nanostructures, J. Phys. D: Appl. Phys. 54 (2021) 505501, http://dx.doi.org/10.1088/1361-6463/ac2110, (12pp).

[4] D.J. Milliron, S.M. Hughes1, Y. Cui1, L. Manna1, J. Li, L.-W. Wang, A.P. Alivisatos1, Colloidal nanocrystal heterostructures with linear and branched topology, Nature 430 (2004) 190–195, http://dx.doi.org/10.1038/nature02695.

[5] X. Rao, et al., Preparation of artificial graphite coated with sodium alginate as a negative electrode material for lithium-ion battery study and its lithium storage properties, Mater. Adv. 3 (2022) 8958–8966, http://dx.doi.org/10.1039/D2MA00820C.

[6] M. Kazes, et al., Lasing from semiconductor quantum rods in a cylindrical microcavity, Adv. Mater. 14 (2002) 317–321, http://dx.doi.org/10.1002/1521-4095(20020219)14:4.

[7] Y. Wang, et al., All inorganic colloidal perovskite quantum dots: a new class of lasing materials with favorable characteristics, Adv. Mater. 27 (2015) 7101, http://dx.doi.org/10.1002/adma.201503573 (8pp).

[8] H. Wang, et al., Perovskite based photodetectors: materials and devices, Chem. Soc. Rev. 46 (2017) 5204–5236, http://dx.doi.org/10.1039/C6CS00896H.

[9] V.V. Nautiyal, P. Silotia, Second harmonic generation in a disk shaped quantum dot in the presence of spin–orbit interaction, Phys. Lett. A 382 (2018) 2061–2068, http://dx.doi.org/10.1016/j.physleta.2018.05.017.

[10] M. Konig, et al., Quantum spin hall insulator state in HgTe quantum wells, Science 318 (2007) 766–770, http://dx.doi.org/10.1126/science.1148047.

[11] J. Sinova, et al., Universal intrinsic spin Hall effect, Phys. Rev. Lett. 92 (2004) 126603, http://dx.doi.org/10.1103/Phys.Rev.Lett.92.126603 (4 pp).

[12] M. Kria, V.V. Nautiyal, K. Lakaal, J. El Hamdaoui, L.M. Pérez, D. Varsha, V. Prasad Laroze, G. Long, E. Feddi, Rashba effect on linear and nonlinear optical properties of a cylindrical core/shell heterojunction quantum dot, J. Front. Phys. 10 (2022) 942758, http://dx.doi.org/10.3389/fphy.2022.942758 (13pp).

[13] D.S. Kumar, S. Mukhopadhyay, A. Chatterjee, Magnetization and susceptibility of a parabolic InAs quantum dot with electron electron and spin orbit interactions in the presence of a magnetic field at finite temperature, J. Magn. Magn. Mater. 418 (2016) 169–174, http://dx.doi.org/10.1016/j.jmmm.2016.02.071.

[14] M.Z. Malik, D.S. Kumar, S. Mukhopadhyay, A. Chatterjee, Role of spin–orbit interactions on the entropy and heat capacity of a quantum dot helium placed in an external magnetic field, Physica E 121 (2020) 114097, http://dx.doi.org/10.1016/j.physe.2020.114097 (7pp).

[15] R. Khordad, Simultaneous effects of electron–electron interactions, Rashba spin–orbit interaction and magnetic field on susceptibility of quantum dots, J. Magn. Magn. Mater. 449 (2018) 510–514, http://dx.doi.org/10.1016/j.jmmm.2017.10.085.

[16] R. Khordad, B. Vaseghi, Magnetic properties in three electrons under Rashba spin orbit interaction and magnetic field, Int. J. Quantum Chem. 119 (2019) e25994, http://dx.doi.org/10.1002/qua.25994 (10 pages).

[17] Y. Khoshbakht, R. Khordad, H.R.R. Sedehi, Magnetic and thermodynamic properties of a nanowire with Rashba spin orbit interaction, J. Low Temp. Phys. 202 (2021) 59–70, http://dx.doi.org/10.1007/s10909-020-02522-2.

[18] V. Nautiyal, D. Munjal, P. Silotia, Spin orbit effect in a quantum dot confined in a Kratzer potential, J. Magn. Magn. Mater. 528 (2021) 167688, http://dx.doi.org/10.1016/j.jmmm.2020.167688 (9pp).

[19] K. Lakaal, M. Kria, J. El Hamdaoui, Varsha, V. Prasad, Vijit V. Nautiyal, M. El-Yadri, L.M. Pérez, D. Laroze, E. Feddi, Polaronic corrections on magnetization and thermodynamic properties of electron electron in 2D systems with rashba spin orbit coupling, J. Magn. Magn. Mater. 551 (2022) 169042, http://dx.doi.org/10.1016/j.jmmm.2022.169042, (10pp).

[20] C.M. Lee, C.C. Lam, S.W. Gu, Low-lying energy spectrum of a magnetopolaron bound to a Coulomb impurity in a quantum dot, Solid State Commun. 112 (1999) 555–560, http://dx.doi.org/10.1016/S0038-1098(99)00398-1.

[21] C.M. Lee, S.W. Gu, Polaron effect on energy spectrum in two-electron quantum dot under magnetic field, Solid State Commun. 116 (2000) 51–56, http://dx.doi.org/10.1016/S0038-1098(00)00279-9.

[22] H. Hassanabadi, H. Rahimov, S. Zarrinkamar, [Html] Rashba coupling in three electron-quantum dot under cylindrical symmetry: An exact solution, Ann. Physics 326 (2011) 2957–2962, http://dx.doi.org/10.1016/j.aop.2011.07.011.

[23] C.M. Lee, Polaron effect on the low-lying states of a three electron quantum dot in a magnetic field, Phys. Rev. B 62 (2000) 4661–4665, http://dx.doi.org/10.1103/PhysRevB.62.4661.

[24] H. Ohno, Making nonmagnetic semiconductors ferromagnetic, Science 281 (1998) 951–956, http://dx.doi.org/10.1126/science.281.5379.95.

[25] R. Flederling, M. Kelm, G. Reuscher, W. Ossau, G. Schmidt, A. Waag, L.W. Molenkamp, Injection and detection of a spin-polarized current in a light emitting diode, Nature 402 (1999) 787–789, http://dx.doi.org/10.1038/45502.

[26] Y. Ohno, D.K. Young, B. Beschoten, F. Matsukura, H. Ohno, D.D. Awschalom, Electrical spin injection in a ferromagnetic semiconductor heterostructure, Nature 402 (1999) 790–792, http://dx.doi.org/10.1038/45509.

[27] H. Ohno, Properties of ferromagnetic III V semiconductors, J. Magn. Magn. Mater. 200 (1999) 110–129, http://dx.doi.org/10.1016/S0304-8853(99)00444-8.

[28] T. Dietl, H. Ohno, F. Matsukura, J. Cibert, D. Ferrand, Zener model description of ferromagnetism in zinc blende magnetic semiconductors, Science 287 (2000) 1019–1022, http://dx.doi.org/10.1126/science.287.5455.1019.

[29] D.P. DiVincenzo, Quantum computing and single-qubit measurements using the spin filter effect, J. Appl. Phys. 85 (1999) 4785–4787, http://dx.doi.org/10.1063/1.370481.

[30] A. Manchon, H.C. Koo, J. Nitta, S.M. Frolov, R.A. Duine, New perspectives for Rashba spin orbit coupling, Nat. Mater. 14 (2015) 871–882, http://dx.doi.org/10.1038/nmat4360.

[31] S.I. Pekar, Research on Electron Theory of Crystals, AEC, Division of Technical Information, Washington, D. C, 1963;
S.I. Pekar, Untersuchungen uber die Elektronentheorie der Kristalle, Akademie-Verlag, Berlin, 1954.

[32] T.D. Lee, F.E. Low, D. Pines, The motion of slow electrons in a polar crystal, Phys. Rev. 90 (1953) 297–302, http://dx.doi.org/10.1103/PhysRev.90.297.

[33] Y.F. Huangfu, Z.W. Yan, Bound polaron in a spherical quantum dot under an electric field, Physica E 40 (2008) 2982–2987, http://dx.doi.org/10.1016/j.physe.2008.02.020.

[34] D.V. Melnikov W.B. Fowler, Bound polaron in a spherical quantum dot: The all coupling variational approach, Phys. Rev. B 64 (2001) 195335, http://dx.doi.org/10.1103/PhysRevB.64.195335 (12pp).

[35] A. Nazir, D.P.S. McCutcheon, Modelling exciton phonon interactions in optically driven quantum dots, J. Phys.: Condens. Matter 28 (2016) 103002, http://dx.doi.org/10.1088/0953-8984/28/10/103002 (26pp).

[36] E. Feddi, M. El Haouari, E. Assaid, B. Stébé, J. El Khamkhami, F. Dujardin, Magnetic field effect on the polarizability of bound polarons in quantum nanocrystallites, Phys. Rev. B 68 (2003) 235313, http://dx.doi.org/10.1103/PhysRevB.68.235313 (8pp).

[37] J. El Khamkhami, E. Feddi, E. Assaid, F. Dujardin, B. Stébé, M. El Haouari, Magneto bound polaron in CdSe spherical quantum dots: strong coupling approach, Physica E 25 (2005) 366–373, http://dx.doi.org/10.1016/j.physe.2004.06.059.

[38] M. El Haouari, E. Feddi, F. Dujardin, R.L. Restrepo, M.E. Mora-Ramos, C.A. Duque, Polaronic effects on the off–center donor impurity in AlAs/GaAs/SiO2 spherical core/shell quantum dots, Superlattices Microstruct. 111 (2017) 457–465, http://dx.doi.org/10.1016/j.spmi.2017.06.059.

[39] V.K. Pecharsky, K.A. Gschneidner Jr., Magnetocaloric effect and magnetic refrigeration, J. Magn. Magn. Mater. 200 (1999) 44–56, http://dx.doi.org/10.1016/S0304-8853(99)00397-2.
[40] K.A. Gschneidner Jr., A.O. Pecharsky, V.K. Tsoko, Recent developments in magnetocaloric materials, Rep. Progr. Phys. 68 (2005) 1479–1539, http://dx.doi.org/10.1088/0034-4885/68/6/R04.
[41] H.R. Sedehi, R. Khordad, Magnetocaloric effect, magnetic susceptibility and specific heat of tuned quantum dot/ring systems, Physica E 134 (2021) 114886, http://dx.doi.org/10.1016/j.physe.2021.114886 (6pp).
[42] C.O. Edet, P.O. Amadi, E.B. Ettah, N. Ali, M. Asjad, A.N. Ikot, The magnetocaloric effect, thermo-magnetic and transport properties of LiH diatomic molecule, Mol. Phys. 120 (2022) e2059025, http://dx.doi.org/10.1080/00268976.2022.2059025, (12 pp).
[43] H. Fröhlich, et al., XX properties of slow electrons in polar materials, Phil. Mag. 41 (1950) 221–242, http://dx.doi.org/10.1080/14786445008521794.
[44] R.P. Feynman, Slow electrons in a polar crystal, Phys. Rev. 97 (1955) 660–665, http://dx.doi.org/10.1103/PhysRev.97.660.
[45] H. Hassanabadi, M. Solaimani, H. Rahimov, Rashba coupling in three-electron-quantum dot: A numerical solution, Solid State Commun. 151 (2011) 1962–1967, http://dx.doi.org/10.1016/j.ssc.2011.09.009.
[46] H. Hassanabadi, H. Rahimov, S. Zarrinkamar, Analytical treatment of a three electron quantum dot under Rashba spin orbit interaction, Few Body Systems 52 (2012) 87–95, http://dx.doi.org/10.1007/s00601-011-0234-9.
[47] H. Hassanabadi, M. Hamzavi, S. Zarrinkamar, A.A. Rajabi, Quadratic and coulomb terms for the spectrum of a three-electron quantum dot, Few-Body Syst. 48 (2010) 53–58, http://dx.doi.org/10.1007/s00601-010-0092-x.
[48] W. Xie, Polaron effects on linear and nonlinear optical properties of a two-electron quantum dot, Physica B 406 (2011) 1805–1808, http://dx.doi.org/10.1016/j.physb.2011.02.032.
[49] L. Xi Xia, B. Shi Liang, Optical vibration modes and electron phonon interaction in ternary mixed crystals of polar semiconductors, Chin. J. Phys 13 (2004) 71–81, http://dx.doi.org/10.1088/1009-1963/13/1/014.
[50] K.L. Jahan, B. Boyacioglu, A. Chatterjee, Effect of confinement potential shape on the electronic, thermodynamic, magnetic and transport properties of a GaAs quantum dot at finite temperature, Sci. Rep. 9 (2019) 15824, http://dx.doi.org/10.1038/s41598-019-52190-w (10pp).